

Kinking in LPSO Mg-Zn-Y Alloys and Other Layered Materials

V.V. Kaminskii^{1,*}, E. Abe², Y. Kawamura³, L.M. Dorogin¹, A.E. Romanov^{1,4}

¹ Institute of Advanced Data Transfer Systems, ITMO University, Kronverkskiy 49, 197101 Saint-Petersburg, Russia

² Department of Materials Science and Engineering, University of Tokyo, Tokyo 113-8656, Japan

³ Department of Materials Science and Engineering, Kumamoto University, Kumamoto 860-8555, Japan

⁴ Sector Theory of Solids, Ioffe Physical-Technical Institute RAS, Polytechnicheskaya 26, 194021 Saint-Petersburg, Russia

Article history

Received May 19, 2022
Received in revised form
June 05, 2022
Accepted June 05, 2022
Available online June 20, 2022

Abstract

Kink band formation (kinking) in layered materials is reviewed. Metal alloys with a long period stacking ordered structure (LPSO) based on Mg-Zn-Y system along with other layered materials demonstrating laminar structure at various scales are put into focus. Despite the variety of layered materials, most of them have common patterns in formation of kinks during deformation. We consider kinking as a specific mechanism of plastic deformation that is illustrated by experimental and theoretical data accumulated in the academic literature during more than five decades of research.

Keywords: Kink band; Kinking; LPSO; Mg-Zn-Y alloys; Mille-feuille structures

CONTENTS

1. Introduction.....	15
2. Layered materials.....	16
2.1. Classification of layered materials.....	16
2.2. LPSO structures in Mg-Zn-Y alloys.....	16
3. Kinking as specific deformation mechanism in layered materials.....	17
3.1. Millimeter scale.....	17
3.2. Micron scale.....	18
3.3. Nanometer scale.....	19
4. Kink formation in LPSO Mg-Zn-Y alloys: experimental facts.....	19
4.1. Types of observed kinks in LPSO Mg-Zn-Y alloys.....	19
4.2. Initial stage of kink formation with dislocation sub-boundaries.....	20
4.3. Stage of macroscopic kinking.....	22
5. Theoretical models for kinking phenomena.....	23
5.1. Early models.....	23
5.2. Geometrical models.....	24
5.3. Molecular dynamics models.....	25
5.4. Dislocation models.....	26
5.5. Disclination models.....	27
6. Conclusions.....	28
Acknowledgements.....	28
References.....	28

1. INTRODUCTION

Layered materials are widespread in nature, for example, in the form of rocks [1], micas [2], wood [3] and in an artificial metal or non-metal composites [4–10]. In contrast to the natural materials, e.g., mica, with the elementary layer thickness on the macroscopic scale, artificial materials, e.g., alloys with long period stacking ordered (LPSO) structure, demonstrate few nanometers layer thickness [11]. In the recent decades, special interest in layered structures of metallic origin increased due to their remarkable physical and mechanical properties, for example high strength [12]. The reason for the high strength of these alloys lays in the development of special type of deformation in them known as the formation of kinks or just kinking. This type of deformation is a feature of the materials with pronounced anisotropy of plastic properties and was first described in the 40s of the last century in single-crystal samples of zinc and cadmium [13]. Later its predominant value for the mechanical properties of Mg-Zn-Y alloys was revealed [14–19].

The purpose of this review is to consider kinking phenomenon and demonstrate the examples of its realization in layered materials. The review is focused on two issues: first, we analyze experimental data on kinking in layered materials and demonstrate its importance for LPSO structures; second, we consider existing theoretical approaches and models for the description of kinking

* Corresponding author: V.V. Kaminskii, e-mail: vvkaminskii@itmo.ru

phenomenon. The review starts with a short introduction. Classification and examples of layered materials are given in Section 2. In Section 3, we consider kinking as a specific mechanism of plastic deformation in layered materials and discuss the common features being peculiar to kinking in various materials. In Section 4, we give a short overview on kink development in materials with LPSO structure that includes the description of the nomenclature of the kinks observed and facts on their contribution to the strength characteristics of the materials. Section 5 presents theoretical models describing the process of kink formation and development, from the early models of the late 40s of the last century to the most recent ones such as ripplocation and disclination models. In the Section 6, we summarize the main points of the review.

2. LAYERED MATERIALS

In general case, a layer can be defined as a physical object of a finite thickness with two other lateral dimensions much larger than the above thickness. Layers that form layered materials can originate because of energy benefits as a result of self-organization bottom-up processes, which, e.g., take place in LPSO and eutectic composite materials, or can be created in top-down processes, e.g., when gluing the stack of plates. Mille-feuille structures also present a scientific interest, for which hard and soft layers are stacked [20,21].

2.1. Classification of layered materials

A large variety of layered materials known today may demonstrate a big difference in the thickness of an individual layer, while having the common features in the development of kinking in the process of their deforming; see Fig. 1. From the point of view of features, the formation of kinks makes sense to divide by the size of the elementary layer. Below in the article we will talk about layered materials whose size of one layer does not exceed a fraction of a millimeter.

Millimeter scale $\sim(0.1-1)$ mm. Artificial composite materials are often fabricated with millimeter scale layer thickness. It is convenient to use, for example, sheets of paper or textolite (composite epoxy material) glued under a press to demonstrate the phenomenon of kinking itself [10]. Natural materials such as mica also exhibit millimeter scale layer dimensions [2].

Micron scale $\sim(0.1-10)$ μ m. Wide varieties of layered materials have micron-sized layer dimensions. Examples of materials from this category include: wood; titanium aluminide and Cu-Nb alloys [6], pyrolytic graphite [9], eutectic alloys [8].

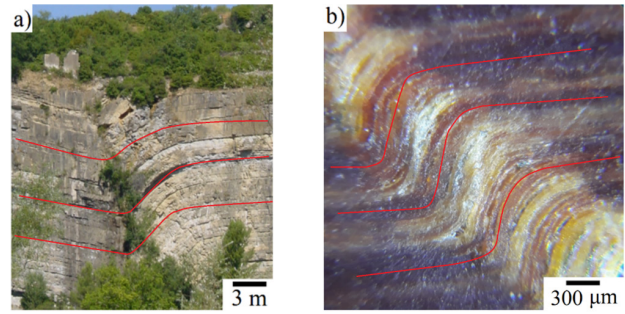


Fig. 1. Examples of kink band formation of different length scales: (a) Tectonic break with a kink band (adapted from Ref. [22]); (b) kink band in artificial textolite based composite material fabricated in 1960s at Ioffe Institute, Leningrad, USSR.

Nanometer scale $\sim(1-10)$ nm. Layered materials with nanometer dimensions include MAX phases [5]. These are materials with the composition formula: $Mz+1AXz$, (MAX), which are layered hexagonal nitrides and carbides. In this formula, $z = 1$ to 4, M is a transition metal, A is a group (often IIIA, IVA) of the element, X is either nitrogen or carbon. Another unique material with a layered structure, which will be discussed further, is Mg based alloy with LPSO structure [12,23,24].

2.2. LPSO structures in Mg-Zn-Y alloys

LPSO structure was discovered by Kawamura et al. in 2001 [12] when the $Mg_{97}Y_2Zn_1$ (at %) alloy was fabricated by rapidly solidified powder metallurgy processing. Further investigation found that this alloy possessed an extremely high yield strength of 610 MPa and a 5% elongation at room temperature. Later on, extruded $Mg_{97}Zn_1Y_2$ and $Mg_{96}Zn_2Y_2$ alloys with LPSO structure had been found to exhibit significantly enhanced mechanical properties, such as increased yield strength, compared to the commercial magnesium alloys [14]. Initially, this increase in strength properties was associated with a decrease in grain size. However, as the study showed, the formation of LPSO phases had a key influence on the strength characteristics [15,16]. The LPSO structure is formed by adding zinc and yttrium to the magnesium alloy [25,26]. Even an insignificant addition of zinc and yttrium changes the main mechanism of deformation of magnesium alloys from twinning to a much more energy consuming process — kinking. It was speculated that the key point here is to increase the c/a ratio of lattice parameters in hexagonal crystal structure of the fabricated material above 1.730 that is much higher of the ideal 1.633 value of the close-packed hcp structure; the change of this parameter is responsible for twinning suppression and initiation of kinking [23]. Figure 2 shows scanning electron microscope (SEM) image of a magnesium alloy sample with a hardening LPSO structure.

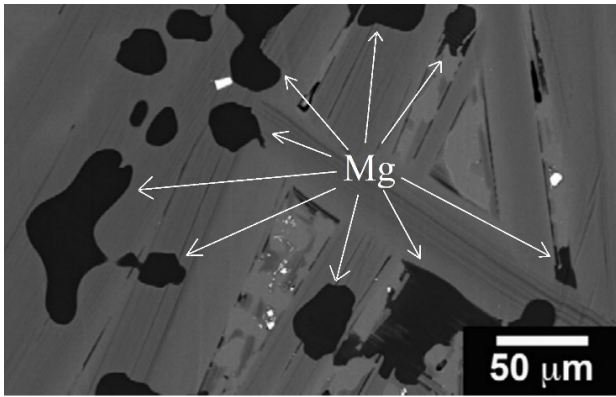


Fig. 2. An artificial layered material. SEM images of the Mg-Zn-Y alloy, where magnesium grains are black and LPSO phases are gray. Adapted from Ref. [24].

There are various types of LPSO structures (10H, 18R, 14H, 24R) detected with the help of scanning transmission electron microscopy (STEM); see Fig. 3. These different types of stacking of atomic layers in an LPSO structure are called polytypes. The alloy with LPSO can have several polytypes at the same time. For example, during extrusion process 18R LPSO structure can be partially or completely transformed into the 14H structure [27]. A remarkable feature of the LPSO structure in comparison with a conventional alloy is the formation of kinks upon deformation of the material.

Later, the structures of the LPSO in the Mg-Zn-RE [28,29], Mg-Y-Cu [30], Mg-Co-Y [31] and Mg-Al-Gd [32]

alloys and their mechanical properties had been demonstrated, with microstructure revealed by the methods of electron microscopy.

3. KINKING AS SPECIFIC DEFORMATION MECHANISM IN LAYERED MATERIALS

The formation of kinks during deformation is typical for most layered materials and has general underlying patterns. Let us consider the geometry of a crystal with kink bands (Fig. 4). It is convenient to break down the kink bands parameters into two groups: internal and external. The first group, for a kink band that has passed through the cross section of the sample, include: the thickness of the kink band H , misorientation between the crystal lattice inside and outside the band θ , and the angle between the boundary of the kink bands and the normal to the acting slip planes outside the kink bands β . The most important of the external geometrical parameters of the kink formation are the orientation of the current slip system of the crystal with regard to the loading axis, the angle between those is χ . Further development of deformation eventually leads to the formation of various ridge kinks, one of which is shown in Fig. 4b.

3.1. Millimeter scale

Another example of the formation of kink bands can be found in artificial composite materials, the examples of

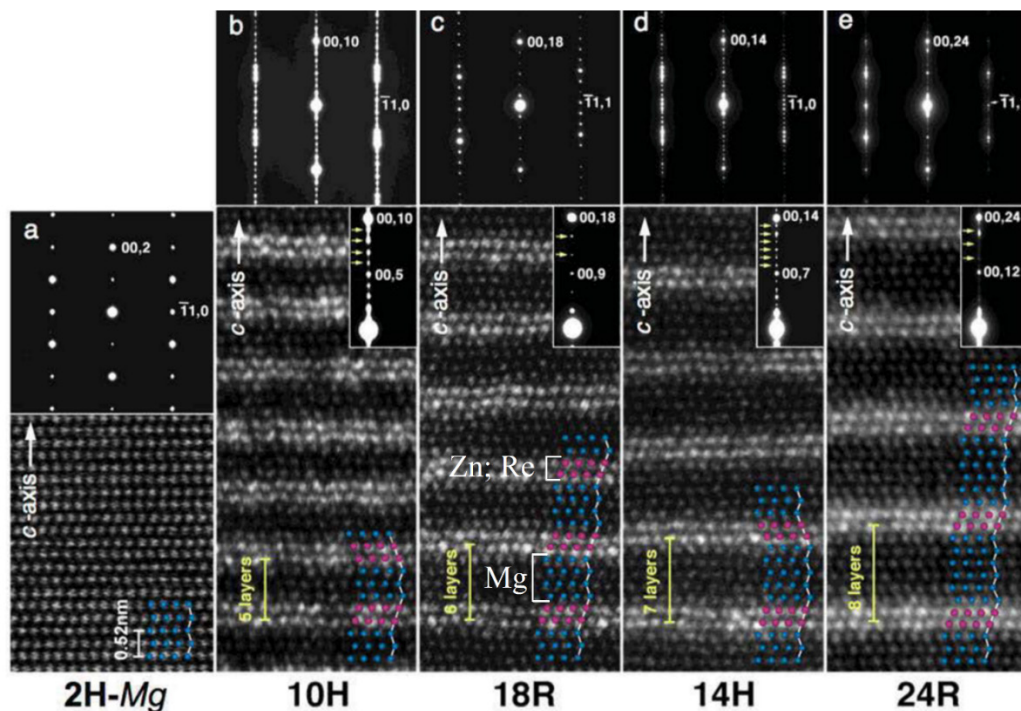


Fig. 3. Classification of highly ordered atomistic layered structure of LPSO materials. STEM images of Mg and LPSO crystals. (a) hcp-Mg, (b) 10H-, (c) 18R-, (d) 14H-, and (e) 24R-LPSO structures. Adapted from Ref. [27].

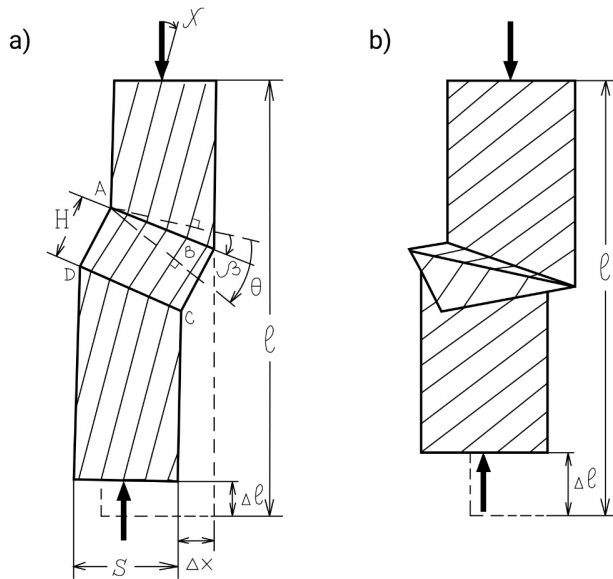


Fig. 4. Geometry of kinking: internal and external parameters. Schematics of the compressed sample with (a) a single kink band; (b) with a ridge kink. H is the thickness of the kink band; θ , β are misorientation angles; χ is the angle between the load axis and the basal slip planes; Δx , Δl show the changes in sample size as a result of loading.

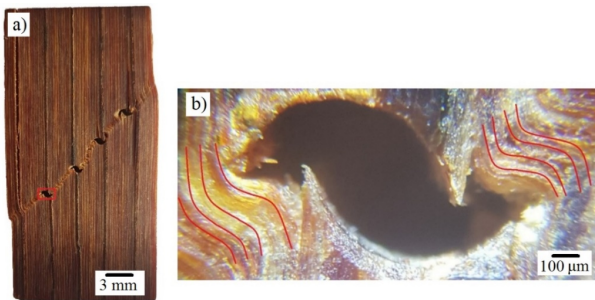


Fig. 5. Kinking in the layered textolite material commonly used in electronics industry and as a structural material fabricated in 1960s at Ioffe Institute, Leningrad, USSR. (a) A textolite bar with the kink band with void defects; (b) zoom-in photograph of the area around a void defect.

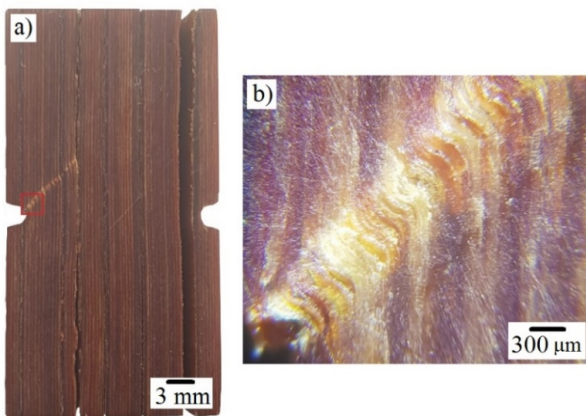


Fig. 6. Kinking in a textolite sample with stress concentrator in the form of a notch. (a) Cross-section of a textolite bar; (b) zoom-in photograph of the area at the notch.

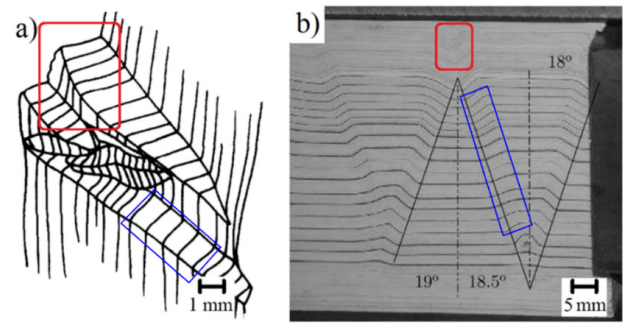


Fig. 7. Illustration of the appearance of kink bands and ridge kinks in layered materials with millimeter scale of lamellas under deformation. Compressed (a) biotite specimen (schematics) and (b) stack of 625 paper sheets (photo). The ridge kinks are marked with red and kink bands with blue rectangles, respectively. Adapted from Refs. [2] and [10].

which are shown in Figs. 5 and 6. The composite material was fabricated by compression and high temperature sintering of textolite plates with thickness of 0.1 to 0.3 mm to form stacks up to 3 mm thick and following gluing of individual stacks [33]. During deformation of the macroscopic rectangular bar sample made of this kind of composite material, various kink bands form. Fig. 5a shows the photo of the sample with a kink band crossing the entire bar. In the place of gluing the stacks, the holes form; see Fig. 5b. Figure 6 shows a stacked textolite sample with a stress concentrator in the form of a notch; the kink band starts at the notch and develops into the bar interior.

Similar scale of lamellas (0.1–0.3 mm) is typical for mica minerals and glued sheets of paper; see Fig. 7. Glued sheets of paper provide a good visual model and have been used to develop theoretical models of kink band formation [10]. Kinking in mica was already known in the 50s of the last century. Mica minerals can be very diverse in their size of lamellae and some of them may extend beyond this scale [2]. On the examples of these objects, in addition to the kink band, one can observe the ridge kinks, which are marked with a red rectangle in both parts of Fig. 7.

3.2. Micron scale

Eutectic alloys provide good examples of this scale. An ideal structure of a eutectic alloy consists of a set of micron thick plates (lamellae) of alternating phases that are parallel to the direction of growth of the sample from the liquid phase [8]. In a typical realistic lamellar material, there are a number of defects in the lamellar structure. An example of materials with such a structure is the eutectic composition Al-CuAl₂; see Fig. 8a. On the transverse sections of eutectic alloy samples, rows of bands or kink bands are very often visible, where lamella traces are wobbling around the growth direction. The development of

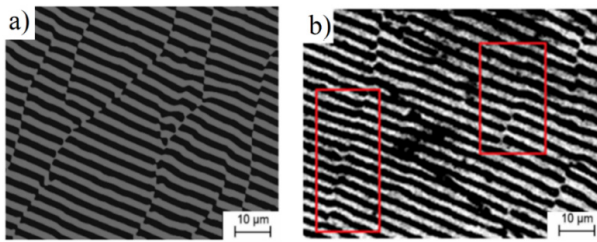


Fig. 8. Optical images of defect structures in eutectic compositions: (a) Al-Al₂Cu (Al – black; Al₂Cu – white) [34]; (b) Sn-Cd (Sn – black; Cd – white), where red rectangles indicate kink bands. Adapted from Ref. [8].

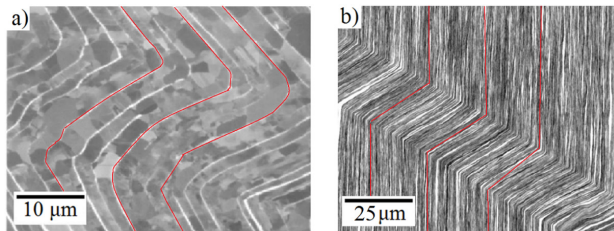


Fig. 9. Metal based composite materials after deformation. (a) SEM image of a Ti-48at%Al-2at%Cr alloy material after deformation; (b) STEM image of a single kink band in Cu-Nb. Adapted from Refs. [6] and [7].

kink bands is realized in the Sn-Cd system and is shown in Fig. 8b [8].

Other layered materials possessing unique physical and mechanical properties are promising composites based on aluminum and titanium. These composite materials are fabricated by different methods with various thickness of lamellas. However, materials with the smallest layer thickness are of a particular interest [6]. Figure 9a depicts the formation of kink bands in the deformation process in aluminum-titanium based composite material. Figure 9b shows another composite with a micro-lamellar structure based on Cu-Nb with a smaller lamella thickness. In this composite, the formation of kink bands is also the main mechanism of deformation, and it was noted that with a decrease in the lamella thickness, the strength of the material increases [7]. In Section 5.2 the analysis of the main characteristics of kink bands will be given for Cu-Nb alloy.

The appearance of kinks band is observed during the mechanical exfoliation of highly oriented pyrolytic graphite (HOPG) [9]. These kink bands are accompanied by mechanical separation of graphite layers (Fig. 10).

3.3. Nanometer scale

LPSO structures and MAX phases are the materials with nanometer scale lamellae. In MAX phases under favorable conditions plasticity is realized in a single interlamellar slip system. In polycrystalline materials with strong plastic anisotropy, large internal stresses and uneven stress distributions develop upon mechanical loading [5].

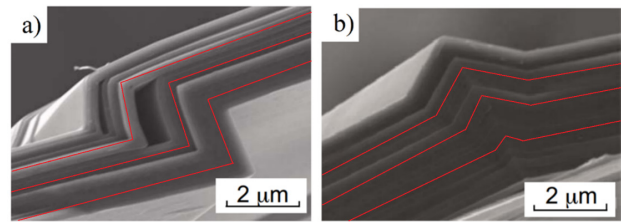


Fig. 10. SEM image illustrating the formation of kinks during peeling graphite flake in highly oriented pyrolytic graphite. (a) Kink band; (b) ridge kink. Adapted from Ref. [9].

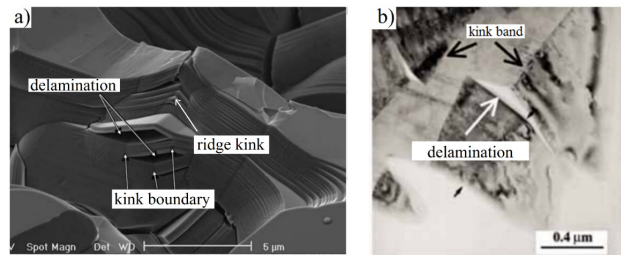


Fig. 11. Delamination in Ti₃SiC₂ layered material (MAX phase) with the formation of ridge kinks and kink bands. (a) SEM and (b) TEM images. Adapted from Refs. [36] and [35].

Favorably oriented grains are deformed via the motion of dislocations in the main slip planes, which quickly transfer the load to grains that are unfavorably oriented with respect to the applied stress. As a consequence of the anisotropy of plastic properties kink bands develop in unfavorably oriented grains. Typical photomicrographs of kink bands in the MAX phases are given in Fig. 11 [35,36]. LPSO structures are considered in the previous and subsequent sections of this review.

4. KINK FORMATION IN LPSO Mg-Zn-Y ALLOYS: EXPERIMENTAL FACTS

4.1. Types of observed kinks in LPSO Mg-Zn-Y alloys

During the deformation of alloys with a LPSO structure, several types of deformation occur, that can also be transformed into each other. In some works, these types are distinguished as kink band, ortho- and ridge kinks [37]. Other works distinguish pre-kink, kink [38], high-angle boundaries [39], and beak-like structures [40]. Despite such a large number of different names for deformation structures, many of them are similar in meaning. It is reasonable to classify the types of related to kinking deformation structures in the following groups. First, low angle kinks (pre-kinks) occur to build individual parts of the kink bands; see selected area A in Fig.12. Second, high angle kinks (planar bands and ortho-kinks), i.e., kinks with sharper edges and with higher angle misorientation boundaries, appear; see selected area B in Fig. 12. During this process, three angular boundaries (1,2,3) are combined

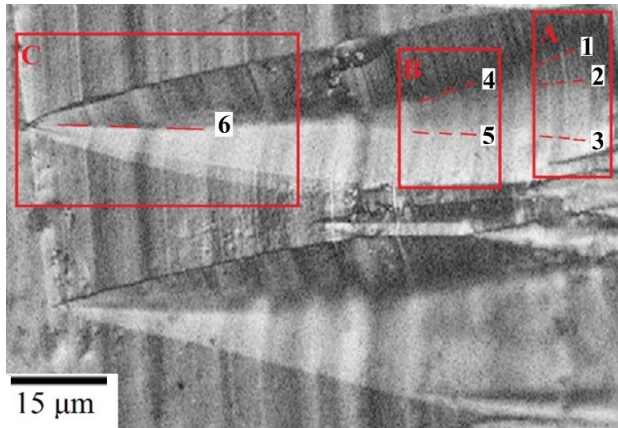


Fig. 12. Optical high magnification image of kinking in a Mg-Zn-Y alloy specimen deformed at room temperature. Explanation of the used designation is given in the text. Adapted from Ref. [23].

into two (4 and 5). Ridge kink (beak-like structure) is the last stage of kink evolution; see selected area C in Fig. 12, which is characterized by the formation of one single sharp central border. During this stage, the creation of two high-angle boundaries (4, 5), and one boundary (6) occurs. This last transformation will be discussed in more details in Section 5.

It is important to note, that all described kink structures are manifestations of the same deformation mechanism. Kinks as three-dimensional structures might present themselves differently depending on the observation angle. For example, it is easy to see from Fig. 13 that an ortho-kink (with two bends) and a simple kink band can be a part of the same structure.

4.2. Initial stage of kink formation with dislocation sub-boundaries

Kinking of all types can be viewed as a phenomenon with a fundamental mechanism spanning across a wide variety of layered materials. Kinking is the result of the anisotropy of plastic deformation being inherent to layered materials.

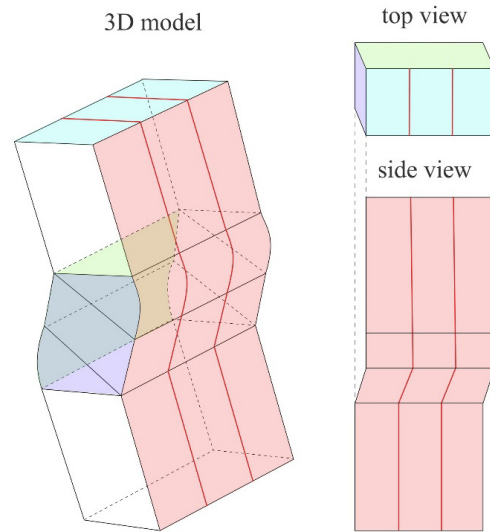


Fig. 13. Schematics of an ortho kink shown in different projections. The red lines indicate layer boundaries.

Symmetric shear stress components in such materials can work only in one of two orthogonal directions. In general, the role of internal stresses lays in the initiation of kink nuclei at various stress concentrators, whereas external loads are responsible for the development of kink band in the material.

The first observations of the formation of kinks in the LPSO structure were made in 2006 [17], but more detailed experimental studies followed later. The origin of kinks has a dislocation nature, and the initial stage of kinking is the formation of pre-kink dislocation sub-boundaries; see Fig. 14, where the sub-boundary under consideration is selected in Fig. 14a. This sub-boundary is the array of edge dislocations (a terminated dislocation wall). Individual dislocations in the array are located at about 20 nm from each other. The formation of a dislocation array leads to disorientation in the structure (Fig. 14b). Further, the development of such disorientations in the materials structure leads to the formation of kinks.

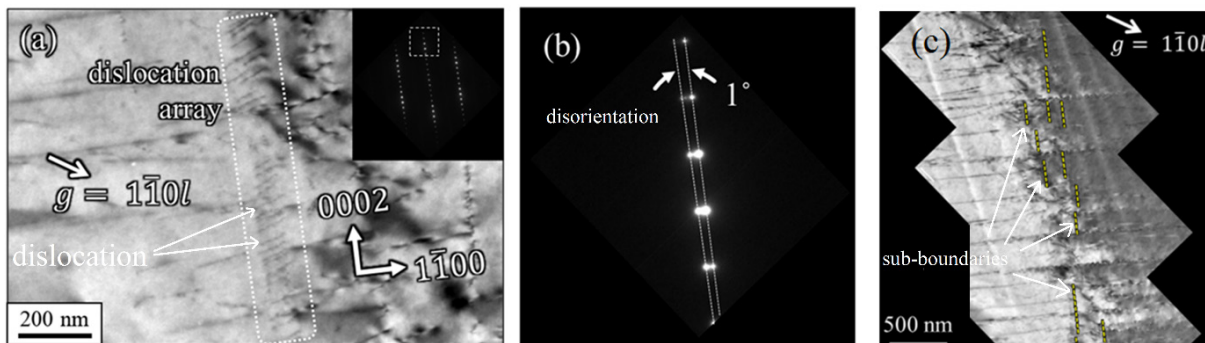


Fig. 14. TEM images of the pre-kink dislocation sub-boundaries in Mg-Zn-Y alloy. (a) Bright field image and (b) corresponding electron diffraction pattern for a single sub-boundary; (c) several dislocation sub-boundaries (designated with yellow dots). Adapted from Ref. [38].

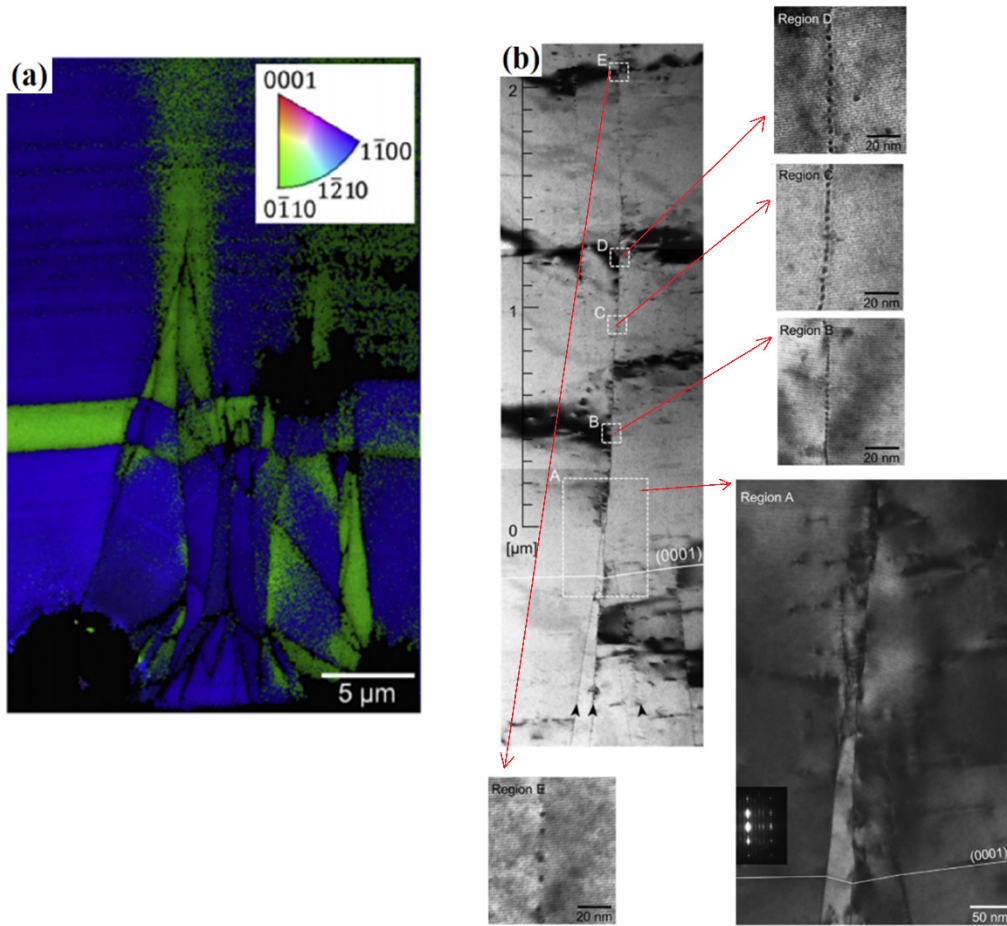


Fig. 15. TEM images of kink formation in Mg-Zn-Y alloy. (a) The tip region of a beak (ridge) shaped kink band; (b) and its front region; designated by arrows insets are bright-field images of regions A, B, C, D, E. Adapted from Ref. [41].

Matsumoto et al. [41] investigated the mechanism of kink band initiation in an 18R-typed LPSO structure performing TEM analysis of the front region of beak-shaped kink bands (or ridge kink). Ridge kink must have at least three kink boundaries, which can be clearly seen in TEM micrographs given in Fig. 15. Outsets in Fig. 15b show in more detail the selected regions. These figures demonstrate how the array of dislocations is gradually transformed into a ridge kink.

Inclusions of another phase have a great influence on kinking in the materials with LPSO structure affecting the process of further deformation of such materials. Inclusions create local stresses that can cause the formation of kinks, even without deformation [42]. The example of a kink band formed in the vicinity of the intermetallic inclusion is shown in Fig. 16. In addition to inclusions, kinking is also affected by heat treatment, e.g., it can manifest as segmentation of kink boundaries [43].

The formation of dislocation boundaries in layered materials can lead to the nucleation of microcracks. In work [44], the mechanism of microcrack formation at two bending boundaries is shown. Alternatively, the formation

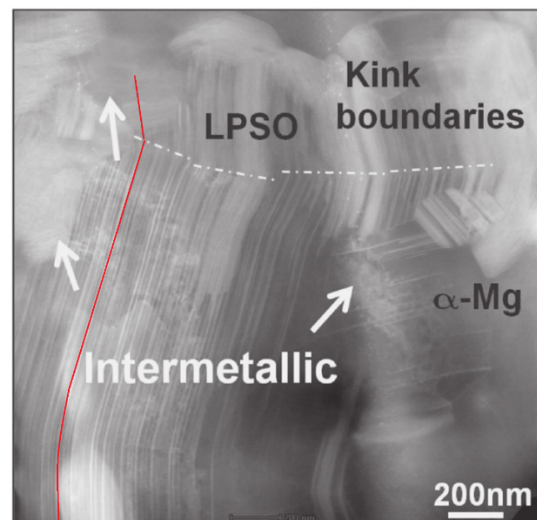


Fig. 16. High-angle annular dark-field imaging-STEM image of the boundaries of the kink (dotted lines) and surrounding intermetallic compounds (marked with white arrows) in magnesium alloy with LPSO structure after extrusion. Adapted from Ref. [42].

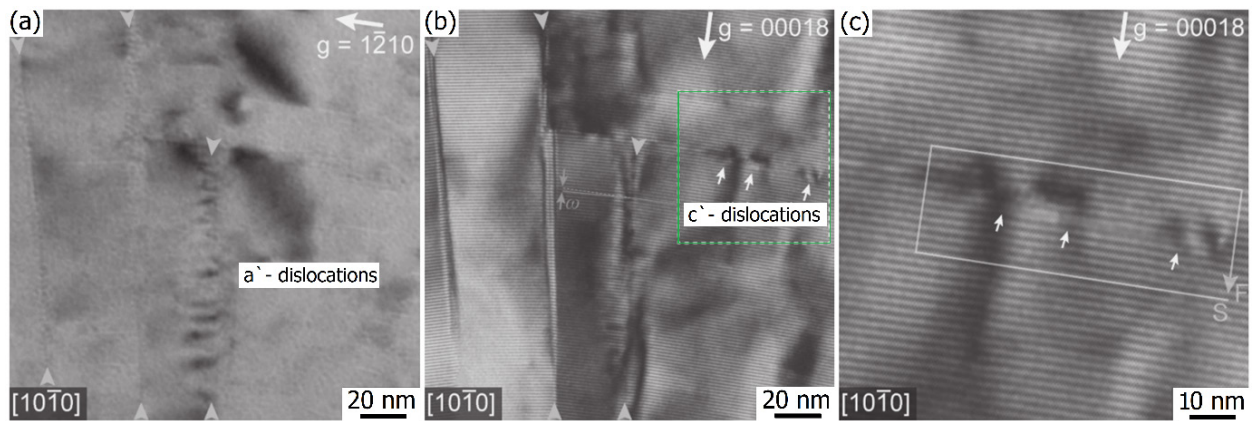


Fig. 17. Bright-field TEM images of the kink interfaces in Mg-Zn-Y with LPSO structure after extrusion; (a) beam condition: $g = 1\bar{2}10$, a' -excitation of the α -Mg structure; (b,c) beam condition: $g = 00018$, c' -excitation of the α -Mg structure. Adapted from Ref. [44].

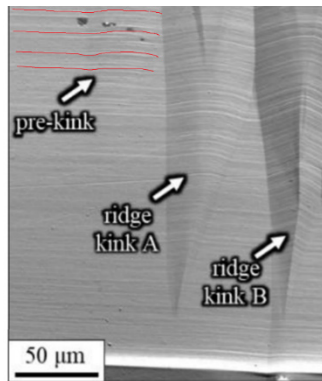


Fig. 18. (a) SEM-SE image of pre-kink and ridge kinks (A, B) in Mg-Zn-Y alloy material. Atomistic layers in the pre-kink are highlighted with red lines. Adapted from Ref. [38].

of a wall of dislocations (sub-boundary) perpendicular to the basal dislocations that form the bending boundaries can be found as internal stresses compensation (Fig. 17).

4.3. Stage of macroscopic kinking

Macroscopic kinking manifests itself as the stage of deformation transformations in a material that can be visible at the micron scale. Examples of such transformations are the ridge kink formations as depicted in Fig. 18 and Fig. 19. In LPSO alloys, ridge kink is always a micron scale structure. The dimensions of this structure, on average, vary over a wide range from 1 μm to 600 μm . With the help of electron microscopy common types of kink deformation in Mg-Zn-Y alloys were revealed in the work of Yamasaki et al. [38]. Ridge kinks are formed from pre-

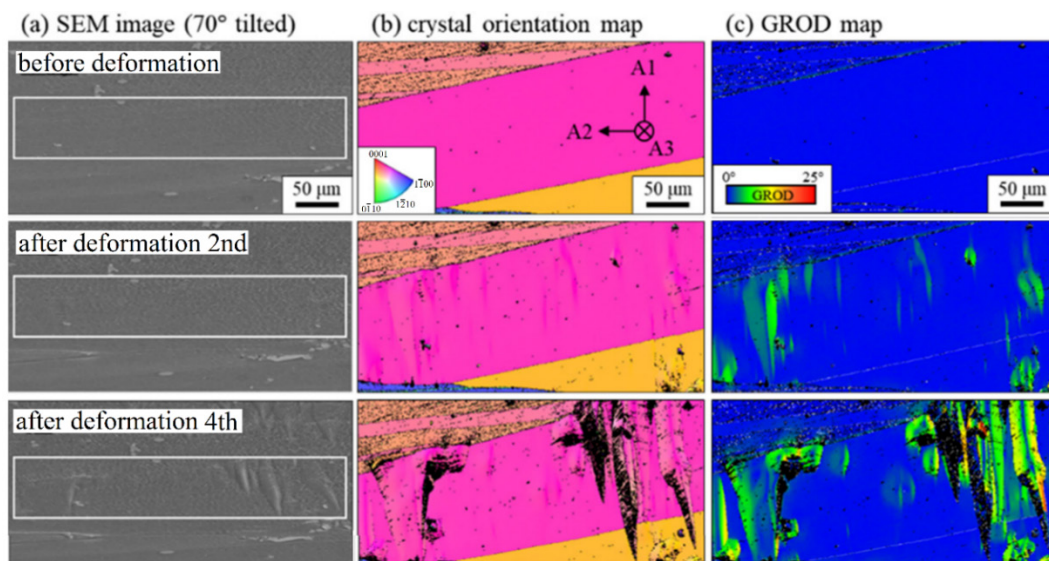


Fig. 19. Evolution of the microstructure of Mg-Zn-Y alloy material under compression (in-situ test in the SEM camera). (a) 70° tilted scanning electron microscope-secondary electrons images, (b) crystal orientation maps indexed from the A3 direction, (c) grain reference orientation deviation (GROD) maps. Adapted from Ref. [38].

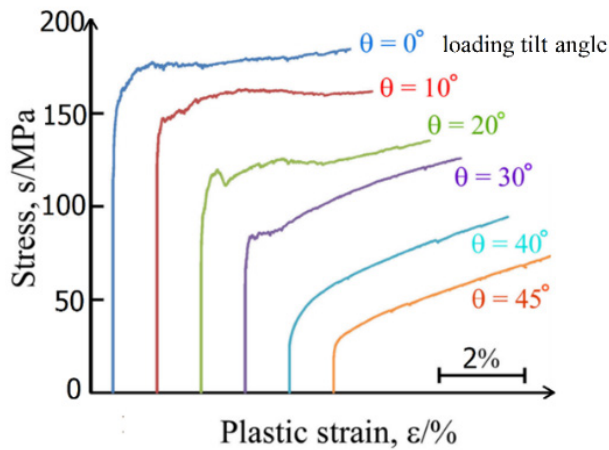


Fig. 20. Stress-strain curves for compression up to 5% plastic strain of Mg-Zn-Y alloy material. Adapted from Ref. [40].

kinks, and pre-kinks, in turn, from the arrays of edge dislocations forming sub-boundaries; see Fig. 18 and Fig. 19.

An experimental illustration of the formation of large ridge kinks up to 600 μm was given in Ref. [40], where the effect of load orientation on the microstructure behavior of polycrystalline rectangular specimens is examined. Six different loading axes were chosen. One was set to be parallel to the growth direction; then, the loading axis was tilted in increments of 10° up to 40° ; see Fig. 20 and Fig. 21. As the inclination angle of the loading axis with respect to the crystal growth direction is increased, the frequency of formation of kink bands in the LPSO-phase direct solidification (DS) crystal monotonically decreases accompanied by a decrease in the yield stress. As it was noted in Ref. [40] kink bands develop macroscopically along a direction approximately perpendicular to grain boundary independent of the loading direction, and basal slip is increased with an increase in the orientation angle (Fig. 21).

5. THEORETICAL MODELS OF KINKING PHENOMENON

5.1. Early models

The first mention about kink formation as a special case of deformation was made in the 40s of the last century. This particular type of deformation was first detected in single-crystal rods of zinc and cadmium by Hess and Barrett [13]. They assumed that the kink band is formed by nucleating pairs of dislocations of opposite signs, as it is shown in Fig. 22.

In terms of dislocations, the essential difference between kinking and other sliding and twinning mechanisms is that sliding requires the generation of a sequence of many dislocations all in the same gliding plane, while

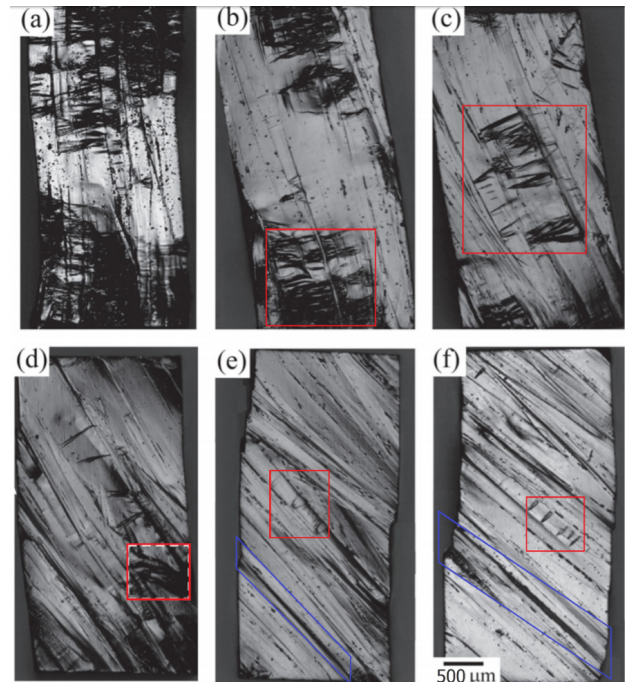


Fig. 21. Optical microscopy images of the Mg-Zn-Y alloy specimens deformed up to 5% plastic strain in the (a) 0° , (b) 10° , (c) 20° , (d) 30° , (e) 40° , and (f) 45° orientations. Adapted from Ref. [40]. Ridge kinks are indicated with red rectangle; basal slip regions — with blue parallelogram.

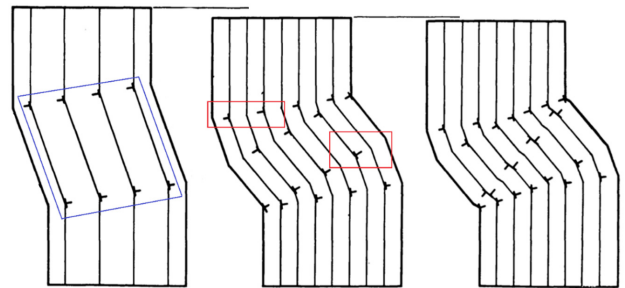


Fig. 22. Dislocation mechanism of kink formation. Nucleation of pairs of edge dislocations followed by dislocation glide. Adapted from Ref. [13]. A kink band is indicated with blue rectangle; a ridge kink — red rectangle.

kinking requires the generation of pairs of dislocations in many parallel gliding planes that are regularly spaced over a small number of atomic distances. In their paper in 1952 [45], Frank and Stroh construct an idealized "kink band" in another ideal crystal subjected to uniform applied stress and show that the kink band can act as a sufficiently effective stress concentrator, expanding itself by generating a new pair dislocation at the edges (Fig. 23). The considered kink band is the region between two approximately flat parallel "walls" of edge dislocations. When the critical value of the deformation is exceeded, the kink band begins to grow, creating new pairs of dislocations at its edge. In addition, this band can decrease upon annihilation of pairs of dislocations.

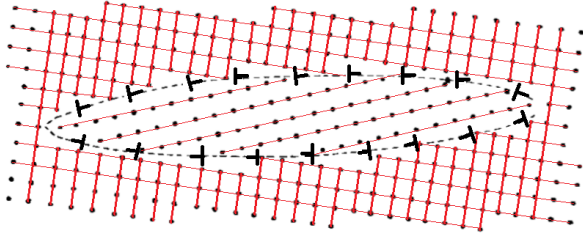


Fig. 23. Diagram shows the atomic configuration and the dislocations in a kink band. Adapted from Ref. [45].

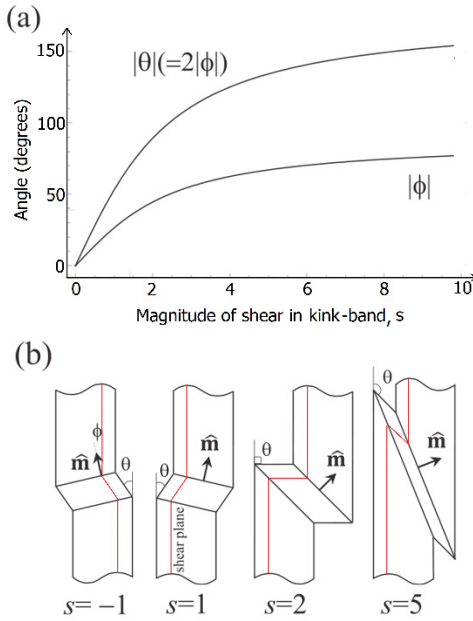


Fig. 24. Shear magnitude dependence of (a) angles of kink band inclination $|\theta|$ and $|\phi|$, and (b) kink band shape viewed for $s = -1, 1, 2,$ and 5 . Angles $|\theta|$ and $|\phi|$ converge to 180° and 90° , respectively, when magnitude of the shear $s \rightarrow \infty$. The kinks are symmetric and the kink plane approaches the shear plane when $\theta = 90^\circ$ at $s = 2$. Adapted from Ref. [37].

5.2. Geometrical models

Geometrical models that determine the relationship between different geometric parameters of kinks give a key to understanding kink deformation and have been investigated in various materials. The strain gradient within the kink is uniform on average and the strain is continuous in the kink plane. These characteristics of the interface are the same as those of the habit plane of martensite and are known as the ‘rank-1 connection’ or ‘invariant plane’ [37]. Based on rank-1 connection the kinematical relationship between the geometric parameters that characterize kink bands, ridge kinks, ortho kinks, and their connections had been revealed. It can be also noted that the disclination type of defect presents a useful theoretical concept for studying kink band connections. Owing to the simple geometry of the kinks, geometrical orientation of the kink plane and the crystallographic rotation angle of a

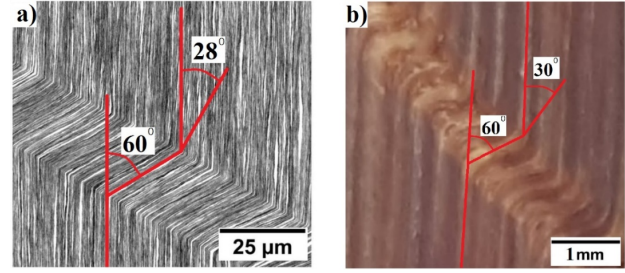


Fig. 25. Correspondence of experimental data with calculation of $|\theta|$ and $|\phi|$ kink band inclination angles: (a) SEM Cu-Nb nanolaminates, (b) optical image of deformed commercial textolite plates. Adapted from Ref. [7].

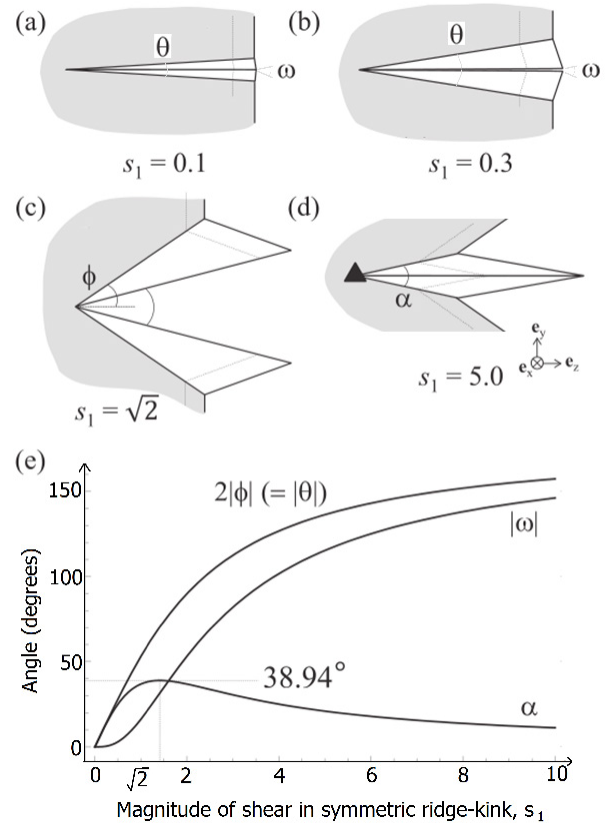


Fig. 26. Morphology of the symmetric ridge kink for (a) $s_1 = 0.1$, (b) $s_1 = 0.3$, (c) $s_1 = \sqrt{2}$, (d) $s_1 = 5.0$, and (e) dependence of s_1 on $2|\phi|$, rotation angles $|\omega|$ and α . The maximum apex angle of the symmetric ridge kink is at $s_1 = \sqrt{2}$. Adapted from Ref. [37].

kink band were determined in analytic forms as functions of the magnitude of shear inside kinks. Figure 24 shows, depending on the magnitude of the shear (s), the angle of inclination (θ and ϕ) of the kink band.

The authors in Ref. [37] compared their theoretical findings with experimental data of work [7] and obtained close values. This can be seen by comparing Fig. 25a,b with graph in Fig. 24a. Similar angle values $|\theta|$ and $|\phi|$ appeared in bars of textolite plates; see Fig. 25b. The geometrical models and analogous calculations can be applied to ridge kinks; see Fig. 26.

5.3. Molecular dynamics models

Molecular dynamics (MD) is a computer simulation method used to determine the stable configurations and dynamics of atoms and molecules. In this method, atoms and molecules are allowed to interact with each other for a fixed time and this gives an idea of the evolution of the entire system of particles, i.e., atoms or molecules. For each atom and molecule, the trajectories of motion are calculated based on the solution of the equations of particle interaction. In work [46], on the basis of this method, the LPSO phases were analyzed, or rather, their behavior during deformation. These LPSO phases were of various types: 24R, 14H, 18R, 10H under various conditions. It was evident from the simulations that deformation twinning was strongly inhibited in the LPSO phase. In the follow-up paper [47], the authors employed a large-scale model to reduce the influence of artificial deformation constraints and provided an analysis of the slip system acting during the kink deformation process of the LPSO phase (Fig. 27).

For research of deformation mechanism of ridge-shaped kink structure in layered solids Lei and Nakatani used spring–mass simulation [48]; see Fig. 28. The motion of particles is numerically modeled as a two-dimensional dynamics problem with a mixed force field, containing harmonic, Morse and angle interaction potentials. As a result, with changing the parameters in the equations for different cases (for example, to study the effect of stiffness

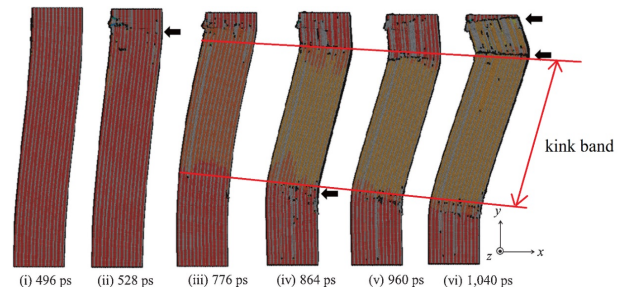


Fig. 27. Deformation of LPSO alloy with structural changes evolution as a function of time in picoseconds (ps), numerically simulated with molecular dynamics simulation. Atoms shown in black and gray are defect atoms. The hcp-structured atoms are colored according to the local c-axis direction, i.e., red indicate the angles between the projection vector of the c-axis on the xy-plane and x-axis direction are 0° and green 45° . Continuous RGB (red, green, blue) coloring is used for intermediate angles. Adapted from Ref. [47].

on bending) the snapshots shown in Fig. 29 were delivered. This model was proved to be suitable for modeling layered materials; in particular, in its framework Ti_2SiC and LPSO simulations were performed [49].

A few years ago, a new term appeared in the theory of the development of deformations in layered materials, namely, the mechanism of ripplocations [50–54]. Ripplocations are line defects, similar to dislocations in van der Waals (vdW) layers, which possess crystallographic Burgers vector as ordinary dislocations but feature “surface ripples” due to the ease of bending and weak vdW adhesion of the atomic layers. If the delamination mechanism in

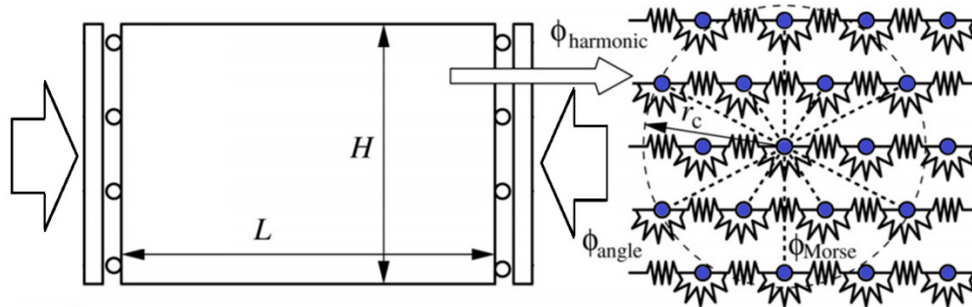


Fig. 28. Spring–mass model used for computational simulations of uniaxial compression tests. The model consists of N particles of mass m in the area specified by the geometry width L and height H . Adapted from Ref. [48].

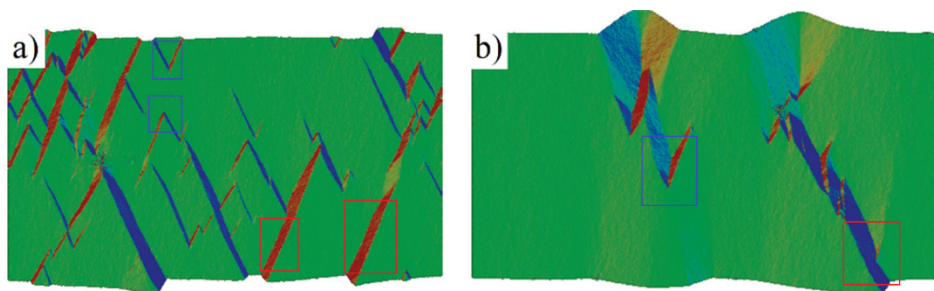


Fig. 29. Spring-mass dynamics simulation of deformation of LPSO. (a) and (b) are snapshots of the particle configuration from the computational simulation for two realizations. Ridge kinks are indicated with blue rectangles, kink bands with red rectangles. Adapted from Ref. [48].

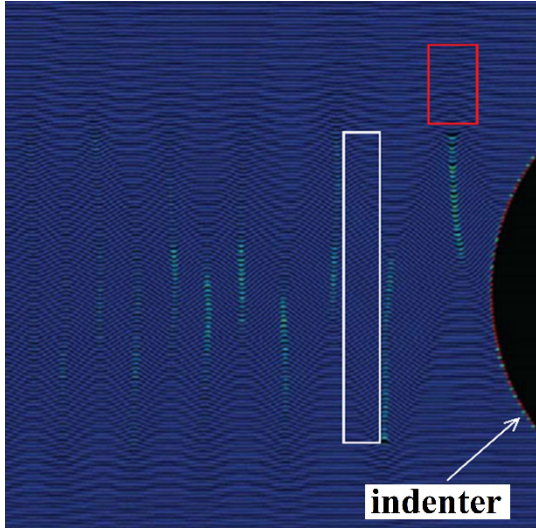


Fig. 30. Molecular dynamics simulation using the ripplocation model of kink bands formation in graphene under deformation (a freeze frame from the video). A kink band is selected with white rectangle; a ridge kink — red rectangle. Adapted from Ref. [53].

vdW layer systems was still understood within the framework of other theories, the ripplocation mechanism had not been well-explained. However, ripplocation type of deformation is often found in MAX phases. For such systems, atomistic MD modeling is performed using the

LAMMPS software [47]. This concept is aimed to explain the formation of ripples and fracture in layered materials. An example of modeling kinks using this method can be seen in Fig. 30.

5.4. Dislocation models

The largest group of models (including early ones mentioned above) describing kinking phenomenon explores a dislocation approach. These models use the movement of dislocations as the basis for the description of kink band formation and development. Dislocations are important defects in crystal lattice, since they can multiply easily and contribute greatly to the distortion of the lattice [55–57], which is the cause of the formation of kinks.

The paper [58] described the model based on dislocations for studying the formation of kinks in LPSO alloys. In the model of crystal plasticity based on dislocations, it is possible to determine the mobility and interaction of dislocations among active glide systems. The model data is based on changes in the dislocation density of the material depending on the strain. An example of using this model for polycrystalline LPSO structure is shown in Fig. 31, where the deformed sample consists of three single crystal strips forming a polycrystal. When the micro-clamped condition is adopted on the grain boundary, the back stress

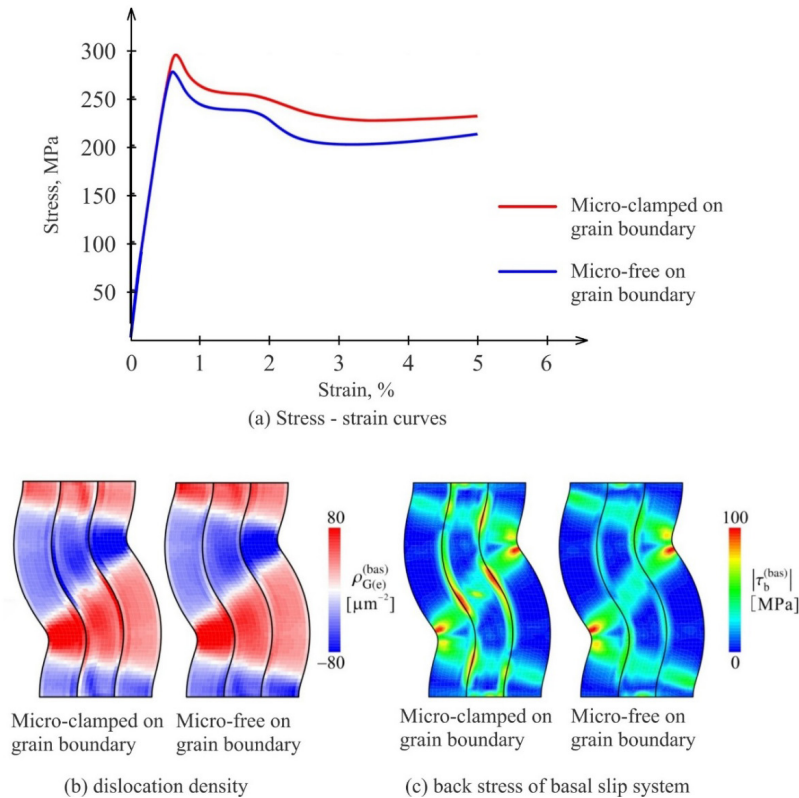


Fig. 31. Compression of a three-layer polycrystal computed with a dislocation-based crystal plasticity model. (a) The stress-strain curve for the two cases when the alloy is clamped at the top and bottom and without clamping; (b) distributions of dislocation density; (c) back stress of basal slip system under micro-clamped and micro-free boundary conditions. Adapted from Ref. [58].

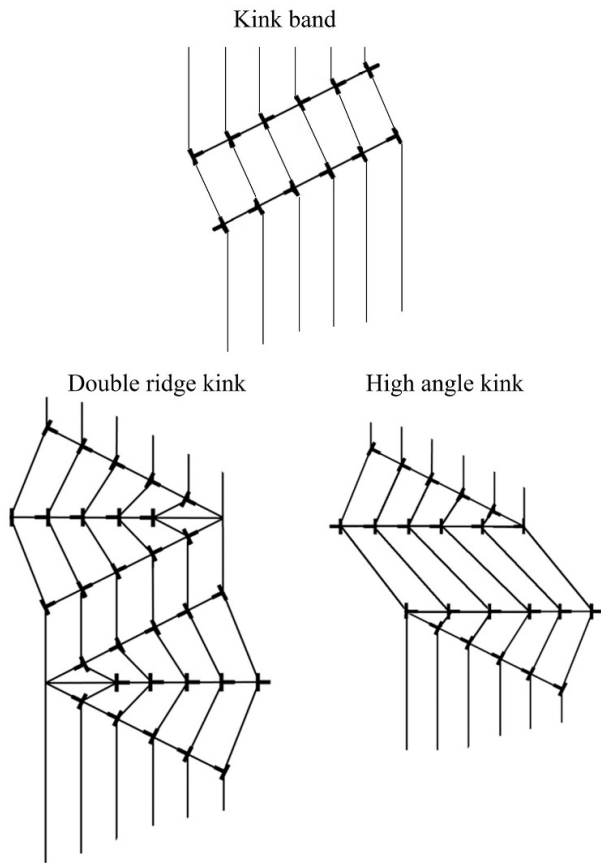


Fig. 32. Scheme of dislocation content for different types of kinks.

becomes large owing to the gradient of geometrically necessary dislocation density near the grain boundary. The growth of back stress leads to the increase of nominal stress.

The mechanism of fracture formation can also be considered using models based on individual dislocations, rather than on the density of dislocations [59]. Each dislocation creates stress field around itself, compressing the lattice on one side, and expanding it on the other. These models make it possible to construct stress fields generated by dislocations. Examples of dislocations in kink structures can be found in Fig. 32.

5.5. Disclination models

It is reasonable to model a kink band as a developing band of misorientation of constant thickness, that gives rise to dislocation-disclination model advanced in 1978 in work [60]. The main idea of the model is that the elastic stresses created by the disclination dipole, make a statistically arranged dislocation ensemble in front of the kink band to be separated into “positive” and “negative” parts whose dislocations, “positive” or “negative”, are caught by the positive or negative disclinations (A and B), respectively (Fig. 33). Each event of capturing a

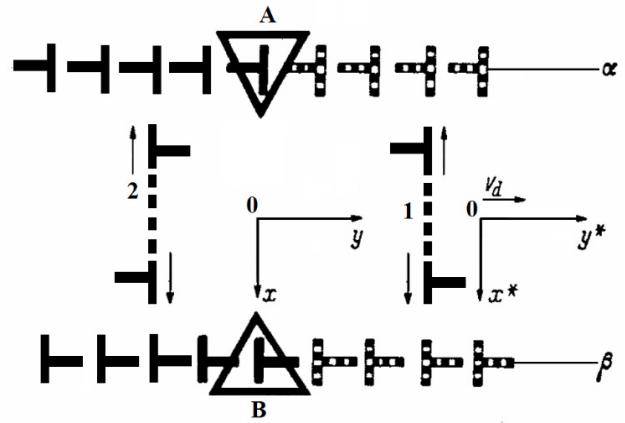


Fig. 33 Dipole of partial wedge disclinations A and B moving in α and β planes, respectively. “1” and “2” are positive and negative gliding dislocation loops that conduct motion of the disclination dipole AB. Adapted from Ref. [60].

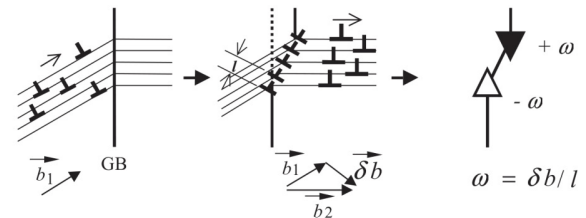


Fig. 34. Formation of grain boundary disclination dipole of strength ω from the flux of edge dislocations towards the grain boundary. Reprinted with permission from Ref. [61].

dislocation dipole by the disclination dipole serves as an elementary act of motion of the kink band.

Consider a later model; see Fig. 34. The shear band consisting of gliding dislocations with Burgers vector \mathbf{b}_1 crosses the grain boundary and is transmitted to a neighboring grain, where the gliding dislocations have Burgers vectors \mathbf{b}_2 . As a consequence, a wall of difference dislocations with Burgers vectors $\delta\mathbf{b} = \mathbf{b}_2 - \mathbf{b}_1$ and interdislocation distance l appears at the intersection together with a grain boundary kink. On the mesoscale, when the characteristic scale of consideration is several orders of magnitude larger than the dimensions of the dislocation wall, the wall can be naturally viewed as a biaxial dipole of grain boundary (GB) wedge partial disclinations with strengths ω .

This model allows one to estimate the yield stress of the crystalline (e.g., metallic) materials. The model assumed that a wedge-disclination dipole with a strength of $\pm\omega$ on a grain boundary splits into a pair of wedge-disclination dipoles under an applied shear stress τ , as shown in Fig. 35. This new split configuration is characterized by the split distance d , the interdislocation spacing l , the dipole arm $2a$ and the disclination strengths $\pm\alpha$ and $\pm\beta$ satisfying the relationships $\beta = b/l$ and $\omega = \alpha + \beta$, where b is the magnitude of Burgers vector for lattice dislocations and ω is the initial strength of the GB disclination dipole.

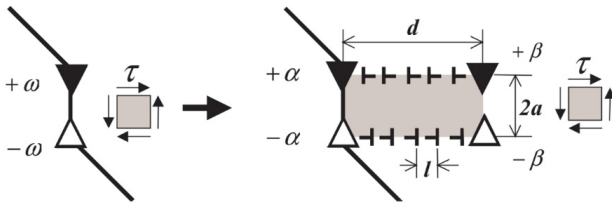


Fig. 35. Disclination-propagation model for kink band development [61].

In fact, the new split disclination configuration represents a model for a kink band of finite length, which consists of a new immobile GB disclination dipole having the strength α (α -dipole), a new mobile disclination dipole with the strength β (β -dipole), and two misorientation boundaries of the length d .

Based on the disclination model [61,62] it becomes possible to estimate yield stress for LPSO phase materials under compression. Using appropriate reference values for disclination strength, kink interface energy, and the kink band width, the critical shear stress can be estimated as $\mu/400$, where μ is the shear modulus. If one adopts the calculated shear modulus of the LPSO phase [63], the critical shear stress for kink formation would result 50 MPa [64].

Disclination-base theoretical models are useful for further understanding of kink-assisted strengthening mechanism [43]. Recent theoretical studies suggest that the disclinations should be introduced during the kink deformation [37] along slip direction and hence may provide extra strengthening through disclinations-dislocations interactions.

6. CONCLUSIONS

Kink band formation (kinking) in layered materials have been briefly overviewed summarizing the experimental and theoretical data on the topic accumulated in the academic literature during more than five decades of research. Kinking deformation mechanism was found to be the reason for the high strength of crystalline materials with a long period stacking ordered structure (LPSO) based on Mg-Zn-Y alloys, which revived interest of scientific community to Mg-based alloys and formed the focus of this paper.

Despite the apparent variety of layered materials with both structural and dimensional differences, most of them have common patterns in formation of kinks during deformation. Different types of kink structures (e.g., kink band, ortho and ridge kinks) can be generally viewed as the same deformation mechanism, while due to their three-dimensional geometry those might present themselves in different shapes (projections) in microscopy imaging. Moreover, kinking can be considered as a specific mechanism of plastic deformation. Several theoretical models were

proposed for describing this mechanism, including simple geometrical models, models based on the methods of molecular dynamics and the models based on the properties of dislocations and disclinations.

In the cases of simplest geometries, such an important parameter as kink orientation can be found in analytical form as a function of the magnitude of shear, but due to the complexity of the defect mechanics in inhomogeneous materials numerical atomistic models are also useful. For example, atomistic simulations enable a detailed study of the mechanics of ripplings — line defects, similar to dislocations in van der Waals layers.

The future line of research in mechanics of layered materials will benefit from the synergy of theoretical approaches at the different scales, including atomistic models, “classical” theory of defects and emerging empirical models inspired by the outcomes of those.

ACKNOWLEDGEMENTS

AER acknowledges the support from Russian Science Foundation under project grant no. 19-19-00617.

REFERENCES

- [1] M.S. Paterson, L.E. Weiss, *Experimental folding in rocks*, Nature, 1962, vol. 195, no. 4846, pp. 1046–1048.
- [2] I. Borg, J. Handin, *Experimental deformation of crystalline rocks*, Tectonophysics, 1966, vol. 3, no. 4, pp. 249–367.
- [3] L. Benabou, *Finite strain analysis of wood species under compressive failure due to kinking*, International Journal of Solids and Structures, 2012, vol. 49, no. 3–4, pp. 408–419.
- [4] J. Kim, S. Sandlobes, D. Raabe, *On the room temperature deformation mechanisms of a Mg–Y–Zn alloy with long-period-stacking ordered structures*, Acta Materialia, 2015, vol. 82, pp. 414–423.
- [5] M.W. Barsoum, L. Farber, T. El-Raghy, *Dislocations, kink bands, and room-temperature plasticity of Ti_3SiC_2* , Metallurgical and Materials Transactions A, 1999, vol. 30, no. 7, pp. 1727–1738.
- [6] T. Schaden, F.D. Fischer, H. Clemens, *Numerical modeling of kinking in lamellar γ -TiAl based alloys*, Advanced Engineering Materials, 2006, vol. 8, no. 11, pp. 1109–1113.
- [7] T. Nizolek, N.A. Mara, I.J. Beyerlein, J.T. Avallone, T.M. Pollock, *Enhanced plasticity via kinking in cubic metallic nanolaminates*, Advanced Engineering Materials, 2014, vol. 17, no. 6, pp. 781–785.
- [8] R. Racek, G. Lesoult, *Ripening of Sn–Cd eutectic microstructures*, Journal of Crystal Growth, 1972, vol. 16, no. 3, pp. 223–226.
- [9] Z. Liu, Q. Zheng, J.Z. Liu, *Stripe kink microstructures formed in mechanical peeling of highly orientated pyrolytic graphite*, Applied Physics Letters, 2010, vol. 96, no. 20, art. no. 201909.
- [10] M.A. Wadee, G. Hunt, M. Peletier, *Kink band instability in layered structures*, Journal of the Mechanics and Physics of Solids, 2004, vol. 52, no. 5, pp. 1071–1091.
- [11] E. Oñorbe, G. Garcés, P. Pérez, *Effect of the LPSO volume fraction on the microstructure and mechanical*

- properties of Mg-Y_{2x}-Zn_x alloys*, Journal of Materials Science, 2012, vol. 47, no. 2, pp. 1085–1093.
- [12] Y. Kawamura, K. Hayashi, A. Inoue, T. Masumoto, *Rapidly solidified powder metallurgy Mg₉₇Zn₁Y₂ alloys with excellent tensile yield strength above 600 MPa*, Materials Transactions, 2001, vol. 42, no. 7, pp. 1172–1176.
- [13] J.B. Hess, C.S. Barrett, *Structure and nature of kink bands in zinc*, Metals Transactions, 1949, vol. 1, no. 9, pp. 599–606.
- [14] Y. Kawamura, S. Yoshimoto, *High strength Mg-Zn-Y alloys with LPSO structure*, Magnesium Technology, Warrendale, PA, 2005.
- [15] A. Inoue, Y. Kawamura, M. Matsushita, K. Hayashi, J. Koike, *Novel hexagonal structure and ultrahigh strength of magnesium solid solution in the Mg-Zn-Y system*, Journal of Materials Research, 2001, vol. 16, no. 7, pp. 1894–1900.
- [16] M. Yamasaki, M. Matsushita, K. Hagihara, H. Izuno, E. Abe, Y. Kawamura, *Highly ordered 10H-type long-period stacking order phase in a Mg-Zn-Y ternary alloy*, Scripta Materialia, 2014, vol. 78–79, pp. 13–16.
- [17] S. Yoshimoto, M. Yamasaki, Y. Kawamura, *Microstructure and mechanical properties of extruded Mg-Zn-Y alloys with 14H long period ordered structure*, Materials Transactions, 2006, vol. 47, no. 4, pp. 959–965.
- [18] W. Jiang, C. Zou, Y. Chen, Z. Wei, *The effect of pressure-induced Mg₆₄Zn₁₅Y₂₁ phase on the mechanical properties of Mg-Zn-Y alloy*, Journal of Alloys and Compounds, 2020, vol. 840, art. no. 155682.
- [19] H. Asgharzadeh, E. Yoon, Y. Chae, H. Kim, T. Lee, *Microstructure and mechanical properties of a Mg-Zn-Y alloy produced by a powder metallurgy route*, Journal of Alloys and Compounds, 2014, vol. 586, S1, pp. S95–S100.
- [20] T. Ohashi, N. Kikuchi, A. Fujimori, *Regularity maintenance properties under deformation of kink-introduced nano-mille-feuille structures derived from interfacial friction*, Journal of Physical Chemistry C, 2021, vol. 125, no. 41, pp. 22766–22777.
- [21] Y. Nawa, T. Hasebe, *FTMP-based kink deformation and strengthening mechanisms for mille-feuille structures*, Materials Science Forum, 2021, vol. 1016, pp. 1019–1023.
- [22] Photo by/de Xavier Hienne. The "faïlle des Causses", a geologic fault in the Grands Causses, as seen from Bédarieux (Hérault, France). This image is provided under two licenses: - GNU Free Documentation License (GFDL), version 1.2 or later - Creative Commons Attribution-ShareAlike (CC-by-SA), version 1.0 or later.
- [23] K. Hagihara, N. Yokotani, Y. Umakoshi, *Plastic deformation behavior of Mg₁₂YZn with 18R long-period stacking ordered structure*, Intermetallics, 2010, vol. 18, no. 2, pp. 267–276.
- [24] M. Yamasaki, K. Hagihara, S. Inoue, J.P. Hadorn, Y. Kawamura, *Crystallographic classification of kink bands in an extruded Mg-Zn-Y alloy using intragranular misorientation axis analysis*, Acta Materialia, 2013, vol. 61, no. 6, pp. 2065–2076.
- [25] E. Abe, Y. Kawamura, K. Hayashi, A. Inoue, *Long-period ordered structure in a high-strength nanocrystalline Mg-1at%Zn-2at%Y alloy studied by atomic-resolution Z-contrast STEM*, Acta Materialia, 2002, vol. 50, no. 15, pp. 3845–3857.
- [26] D.H. Ping, K. Hono, Y. Kawamura, A. Inoue, *Local chemistry of a nanocrystalline high-strength Mg 97 Y 2 Zn 1 alloy*, Philosophical Magazine Letters, 2002, vol. 82, no. 10, pp. 543–551.
- [27] E. Abe, A. Ono, T. Itoi, M. Yamasaki, Y. Kawamura, *Polymorphs of long-period stacking structures synchronized with chemical order in a dilute Mg-Zn-Y alloy*, Philosophical Magazine Letters, 2011, vol. 91, no. 10, pp. 690–696.
- [28] Y. Kawamura, M. Yamasaki, *Formation and mechanical properties of Mg₉₇Zn₁RE₂ alloys with long period stacking ordered structure*, Materials Transactions, 2007, vol. 48, no. 11, pp. 2986–2992.
- [29] D. Egusa, E. Abe, *The structure of long period stacking/order Mg-Zn-RE phases with extended non-stoichiometry ranges*, Acta Materialia, 2012, vol. 60, no. 1, pp. 166–178.
- [30] Y. Kawamura, T. Kasahara, S. Izumi, M. Yamasaki, *Elevated temperature Mg₉₇Y₂Cu₁ alloy with long period ordered structure*, Scripta Materialia, 2006, vol. 55, no. 5, pp. 453–456.
- [31] K. Guan, M. Egami, D. Egusa, H. Kimizuka, M. Yamasaki, Y. Kawamura, E. Abe, *Short-range order clusters in the long-period stacking/order phases with an intrinsic-I type stacking fault in Mg-Co-Y alloys*, Scripta Materialia, 2022, vol. 207, art. no. 114282.
- [32] H. Yokobayashi, K. Kishida, H. Inui, M. Yamasaki, Y. Kawamura, *Enrichment of Gd and Al atoms in quadruple close packed planes and their in-plane long range ordering in the long period stacking ordered phase in the Mg-Al-Gd system*, Acta Materialia, 2011, vol. 59, no. 19, pp. 7287–7299.
- [33] Private communication. Textolite rectangular bars fabricated at the Ioffe Physical-Technical Institute, Leningrad, USSR in 1960s and subjected to compression at room temperature.
- [34] K. Hagihara, T. Tokunaga, K. Nishiura, S. Uemichi, S. Ohsawa, *Control of kink-band formation in mille-feuille structured Al/Al₂Cu eutectic alloys*, Materials Science and Engineering: A, 2021, vol. 825, art. no. 141849.
- [35] M. Radovic, M.W. Barsoum, *MAX phases: bridging the gap between metals and ceramics*, American Ceramic Society Bulletin, 2013, vol. 92, no. 3 pp. 20–27.
- [36] Z. Sun, A. Murugiah, T. Zhen, A. Zhou, M. Barsoum, *Microstructure and mechanical properties of porous Ti₃SiC₂*, Acta Materialia, 2005, vol. 53, no. 16, pp. 4359–4366.
- [37] T. Inamura, *Geometry of kink microstructure analysed by rank-1 connection*, Acta Materialia, 2019, vol. 173, pp. 270–280.
- [38] S. Yamasaki, T. Tokuzumi, W. Li, M. Mitsuhashi, K. Hagihara, T. Fujii, H. Nakashima, *Kink formation process in long-period stacking ordered Mg-Zn-Y alloy*, Acta Materialia, 2020, vol. 195, pp. 25–34.
- [39] H. Gao, K. Ikeda, T. Morikawa, K. Higashida, H. Nakashima, *Analysis of kink boundaries in deformed synchronized long-period stacking ordered magnesium alloys*, Materials Letters, 2015, vol. 146, pp. 30–33.
- [40] K. Hagihara, T. Okamoto, R. Ueyama, M. Yamasaki, Y. Kawamura, T. Nakano, *Loading orientation dependence of the formation behavior of deformation kink bands in the Mg-based long-period stacking ordered (LPSO) phase*, Materials Transaction, 2020, vol. 61, no. 5, pp. 821–827.
- [41] T. Matsumoto, M. Yamasaki, K. Hagihara, Y. Kawamura, *Configuration of dislocations in low-angle kink boundaries formed in a single crystalline long-period stacking ordered Mg-Zn-Y alloy*, Acta Materialia, 2018, vol. 151, pp. 112–124.
- [42] H. Gao, K. Ikeda, T. Morikawa, K. Higashida, H. Nakashima, *Microstructures of long-period stacking*

- ordered phase of Mg–Zn–Y Alloy*, Materials Transactions, 2013, vol. 54, no. 5, pp. 632–635.
- [43] D. Egusa, K. Inoue, Y. Nagai, E. Abe, *Recovery features of kink boundaries upon post-annealing of a hot-extruded Mg–Zn–Y alloy*, Materials Characterization, 2021, vol. 177, art. no. 111153.
- [44] D. Egusa, M. Yamasaki, Y. Kawamura, E. Abe, *Micro-kinking of the long-period stacking order (LPSO) phase in a hot-extruded Mg₉₇Zn₁Y₂ alloy*, Materials Transactions, 2013, vol. 54, no. 5, pp. 698–702.
- [45] F.C. Frank, A.N. Stroh, *On the theory of kinking*, Proceedings of the Physical Society. Section B, 1952, vol. 65, no. 10, pp. 811–821.
- [46] R. Matsumoto, M. Uranagase, N. Miyazaki, *Molecular dynamics analyses of deformation behavior of long-period-stacking-ordered structures*, Materials Transactions, 2013, vol. 54, no. 5, pp. 686–692.
- [47] R. Matsumoto, M. Uranagase, *Deformation analysis of the long-period stacking-ordered phase by using molecular dynamics simulations: kink deformation under compression and kink boundary migration under tensile strain*, Materials Transactions, 2015, vol. 56, no. 7, pp. 957–962.
- [48] X.-W. Lei, A. Nakatani, *A deformation mechanism for ridge-shaped kink structure in layered solids*, Journal of Applied Mechanics, 2015, vol. 82, no. 7, art. no. 071012.
- [49] X.W. Lei, A. Nakatani, *Analysis of kink deformation and delamination behavior in layered ceramics*, Journal of the European Ceramic Society, 2016, vol. 36, no. 9, pp. 2311–2317.
- [50] J. Aslin, E. Mariani, K. Dawson, M. W. Barsoum, *Ripplications provide a new mechanism for the deformation of phyllosilicates in the lithosphere*, Nature Communications, 2019, vol.10, art. no. 686.
- [51] M.W. Barsoum, G.J. Tucker, *Deformation of layered solids: Ripplications not basal dislocations*, Scripta Materialia, 2017, vol. 139, pp. 166–172.
- [52] J. Griggs, A.C. Lang, J. Gruber, G.J. Tucker, M.L. Taheri, M.W. Barsoum, *Spherical nanoindentation, modeling and transmission electron microscopy evidence for ripplications in Ti₃SiC₂*, Acta Materialia, 2017, vol. 131, pp. 141–155.
- [53] J. Gruber, A.C. Lang, J. Griggs, M.L. Taheri, G.J. Tucker, M.W. Barsoum, *Evidence for bulk ripplications in layered solids*, Scientific Reports, 2016, vol. 6, art. no. 33451.
- [54] A. Kushima, X. Qian, P. Zhao, S. Zhang, J. Li, *Ripplications in van der Waals layers*, Nano Letters, 2015, vol. 15, no. 2, pp. 1302–1308.
- [55] F.C. Frank, *The resultant content of dislocations in an arbitrary intercrystalline boundary*, In: Symposium on Plastic Deformation of Crystal Solids, Mellon Institute, Pittsburgh, 1950.
- [56] J.D. Eshelby, *The determination of the elastic field of an ellipsoidal inclusion, and related problems*, Proceedings of the Royal Society A: Mathematical, Physical and Engineering Sciences, 1957, vol. 241, no. 1226, pp. 376–396.
- [57] E. Kröner, *Kontinuumstheorie der Versetzungen und Eigenspannungen*, Springer-Verlag, Berlin, 1958.
- [58] Y. Kimura, R. Ueta, K. Shizawa, *Crystal plasticity FE simulation for kink band formation in Mg-based LPSO phase using dislocation-based higher-order stress model*, Mechanical Engineering Journal, 2020, vol. 7, no. 4, art. no. 19-00612.
- [59] M.Yu. Gutkin, A.E. Romanov, *Straight edge dislocation in a thin two-phase plate I. Elastic stress fields*, Physica Status Solidi (a), 1991, vol. 125, no. 1, pp. 107–125.
- [60] V.I. Vladimirov, A.E. Romanov, *Partial disclination dipole motion under plastic deformation*, Soviet Phys. Solid State, 1978, vol. 20, no. 10, pp. 1795–1796.
- [61] A.E. Romanov, M.Yu. Gutkin, P. Klimanek, *Nucleation of disclination defects and development of misorientation bands at grain boundary junctions*, in: Proceeding of International Conference “Materials Structure and Micromechanics of Fracture - 3” (MSMF-3), ed. by P.P. Sanderá, Brno, Czech Republic, 2001, pp. 494–501.
- [62] M.Yu. Gutkin, A.E. Romanov, P. Klimanek, *Disclination models for misorientation band generation and development*, Solid State Phenomena, 2002, vol. 87, pp. 113–120.
- [63] M. Tane, Y. Nagai, H. Kimizuka, K. Hagihara, Y. Kawamura, *Elastic properties of an Mg–Zn–Y alloy single crystal with a long-period stacking-ordered structure*, Acta Materialia, 2013, vol. 61, no. 17, pp. 6338–6351.
- [64] T. Fujii, A.E. Romanov, *Estimation of kink nucleation stress by a disclination-propagation model*, International Conference "Advanced Materials Week", The 5th Japan-Russian Seminar on Advanced Materials: the structure and mechanisms of plasticity of advanced magnesium alloys and related materials, 2019, pp. 82.

УДК 538.91; 539.3

Сбросообразование в LPSO сплавах системы Mg-Zn-Y и других слоистых материалах

В.В. Каминский¹, Е. Abe², Y. Kawamura³, Л.М. Дорогин¹, А.Е. Романов^{1,4}

¹Институт перспективных систем передачи данных Университета ИТМО, Кронверкский пр., 49, Санкт-Петербург, 197101, Россия

²Department of Materials Science and Engineering, University of Tokyo, Tokyo 113-8656, Japan

³Department of Materials Science and Engineering, Kumamoto University, Kumamoto 860-8555, Japan

⁴Сектор теории твердого тела, Физико-технический институт им. Иоффе РАН, Политехническая 26, Санкт-Петербург, 194021, Россия

Аннотация. В обзоре обсуждается явление формирования и развития полос сброса в слоистых материалах. Особое внимание уделяется металлическим сплавам с длиннопериодной упорядоченной структурой (LPSO) на основе системы Mg-Zn-Y, также рассматриваются и другие слоистые материалы, демонстрирующие ламинарную структуру на различных масштабах. Несмотря на разнообразие слоистых материалов, для большинства из них характерны общие закономерности образования полос сброса при деформировании. Мы рассматриваем сбросообразование как специфический механизм пластической деформации, что иллюстрируется экспериментальными и теоретическими данными, накопленными в академической литературе за более чем пятидесятилетний период исследований.

Ключевые слова: полосы сброса; сбросообразование; LPSO; Mg-Zn-Y сплавы; слоистые структуры